JOURNAL OF NANO- AND ELECTRONIC PHYSICS
Vol. **18** No 1, 01013(7pp) (2026)

ЖУРНАЛ НАНО- ТА ЕЛЕКТРОННОЇ ФІЗИКИ
Том **18** № 1, 01013(7cc) (2026)

OPEN ACCESS

REGULAR ARTICLE

Electrical Conductivity of Thin Films of Copper-Nickel Alloys

V.B. Loboda*, S.M. Khursenko, V.O. Kravchenko, V.M. Zubko

Sumy National Agrarian University, 40021 Sumy, Ukraine

(Received 02 January 2026; revised manuscript received 14 February 2026; published online 25 February 2026)

This paper presents the results of a study of the electrical conductivity of structurally continuous nanocrystalline films of CuNi alloys in a wide range of thicknesses and component concentrations. Alloy films with thicknesses of 50-200 nm were separated from simultaneous separate evaporation of components (copper and nickel) in a vacuum of 10^{-4} Pa. Copper was evaporated from strips of tungsten foil 0.05 mm thick. Nickel was vaporized by the electron-beam method using an electron diode gun. The condensation speed became 0.5-1.5 nm/s. The purity of the evaporated metals was at least 99.98 %. The temperature dependences of the specific electrical resistance of CuNi alloy films for the second and subsequent heating-cooling cycles were virtually identical, indicating complete stabilization of the film samples' properties after the second annealing cycle. To explain the observed specific irreversible decrease in electrical resistance during thermal stabilization of the electrophysical properties of CuNi alloy films, we used the Wend model, which describes the healing of crystal structure defects in the films. Based on this model, the spectra of crystal structure defects in CuNi alloy films were calculated.

Keywords: Thin films, Nanocrystalline films, Alloys, Electrical conductivity, Crystal structure defects, Activation energy for defect healing.

DOI: 10.21272/jnep.18(1).01013 PACS numbers: 61.82.Rx, 73.61. – r

1. INTRODUCTION

Studying the physical properties of thin metal films helps solve a number of fundamental problems in solid-state physics. Furthermore, the prospects for their practical application are also important. The use of thin metal films in recent decades has led to significant progress in microelectronics, high-frequency technology, optoelectronics, optics, and many other areas of modern science and technology. At the same time, a separate branch of solid-state physics – thin-film physics – has emerged.

Films of ferromagnetic metals (Ni, Fe, Co) and their alloys occupy a special place in thin-film physics. This is primarily due to purely scientific questions, the study of which allows us to solve a number of fundamental problems in two-dimensional magnetism. At the same time, a number of applied problems in the fields of nanoelectronics, spintronics, and other fields are also being addressed. In recent years, a number of new fundamental effects have been discovered in film objects based on ferromagnetic metals, such as giant magnetoresistance, colossal magnetoresistance, spin-polarized tunneling, and others. This creates the basis for the development of miniature magnetoelectronic devices, new methods for recording and storing information, and new types of highly sensitive sensors and detectors.

Along with research on films of pure magnetic metals (Ni, Co, Fe) and Cu, the study of films of metal alloys [1-4] and multilayer film structures [5-7] incorporating these metals is promising. Like bulk alloys, alloy films offer a number of advantages over films made of pure metals: by varying the alloy composition, materials with different electrophysical, physicochemical, and performance properties can be obtained.

It should be emphasized that the properties of thin films differ significantly from those of bulk samples. Limiting the dimensions of film objects in one direction, typically along the thickness, leads to the emergence of so-called size effects. In the bulk state, such effects are either weakly expressed or not observed at all.

This paper presents the results of a study of the electrical conductivity of structurally continuous CuNi alloy films over a wide range of thicknesses and component concentrations. To explain the observed irreversible decrease in electrical resistance during thermal stabilization of the electrophysical properties of CuNi alloy films, we used the Wend model of healing defects in the crystal structure of films [8].

2. EXPERIMENTAL METHODOLOGY AND TECHNIQUE

To study the electrical conductivity, film samples were condensed onto a polished glass plate (Fig. 1) with contact pads pre-applied at $T = 600$ K. The method and technique for producing CuNi alloy films are presented in detail in [9].

The glass plate (1) was secured to a copper substrate holder and maintained good thermal contact with it. The substrate temperature was measured using a copper-constantan thermocouple with an accuracy of ± 10 K. To ensure good adhesion of the contact pad to the glass surface,

* Correspondence e-mail: loboda-v@i.ua

Cite this article as: V.B. Loboda et al., *J. Nano- Electron. Phys.* 18 No 1, 01013 (2026) https://doi.org/10.21272/jnep.18(1).01013

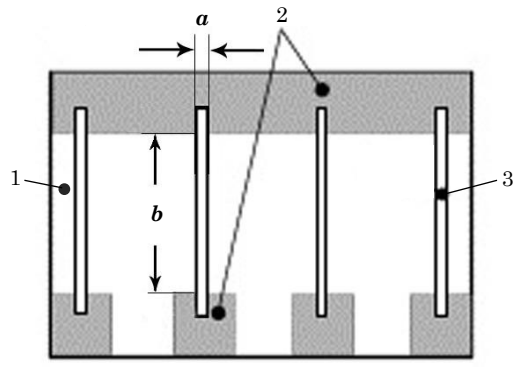

Fig. 1 – Scheme of the substrate with film samples for measuring electrical resistance: 1 – glass plate; 2 – contact pads; 3 – film sample ($a = 2 \pm 0.05$ mm, $b = 10 \pm 0.05$ mm)

the first layer was Cr with a thickness of $d \approx 50$ nm, followed by a second layer of Cu with a thickness of $d = 100$-150 nm, ensuring high electrical conductivity. Fig. 2 shows a series of micrographs of the contact surfaces between the film and the contacts, obtained using a REM-103-01 scanning electron microscope.

The images show the absence of microcracks both at the contact point and in the film samples themselves, which underwent a full thermal stabilization cycle during annealing at 700 K.

Fig. 3 shows the characteristic spectra from the film and contact areas discussed above, allowing us to determine their elemental composition. Localized areas measuring 10 × 10 μm were used to obtain the spectra (for more details, see [10]).

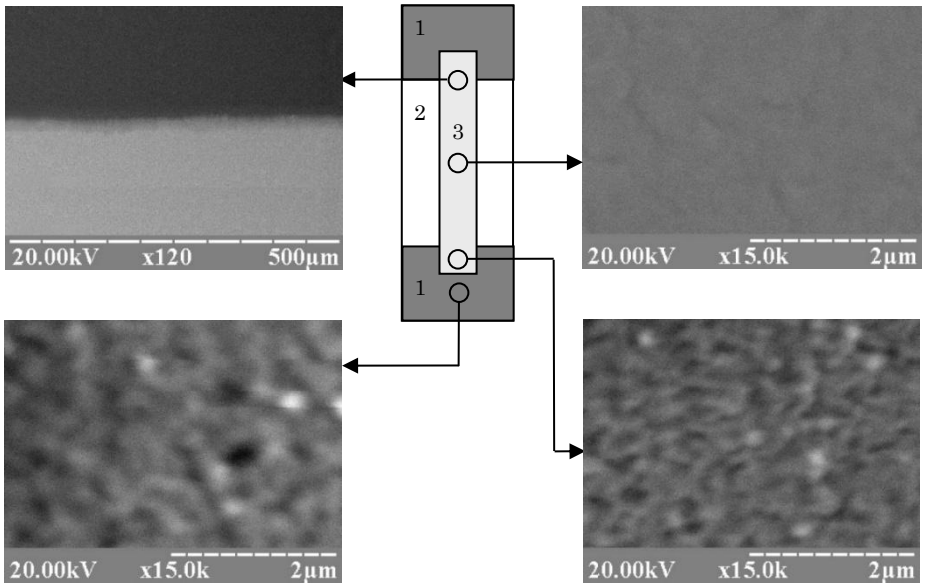

Fig. 2 – Scheme of the film on the substrate and corresponding micrographs of the film and contact areas: 1 – contact pad; 2 – glass substrate, 3 – film

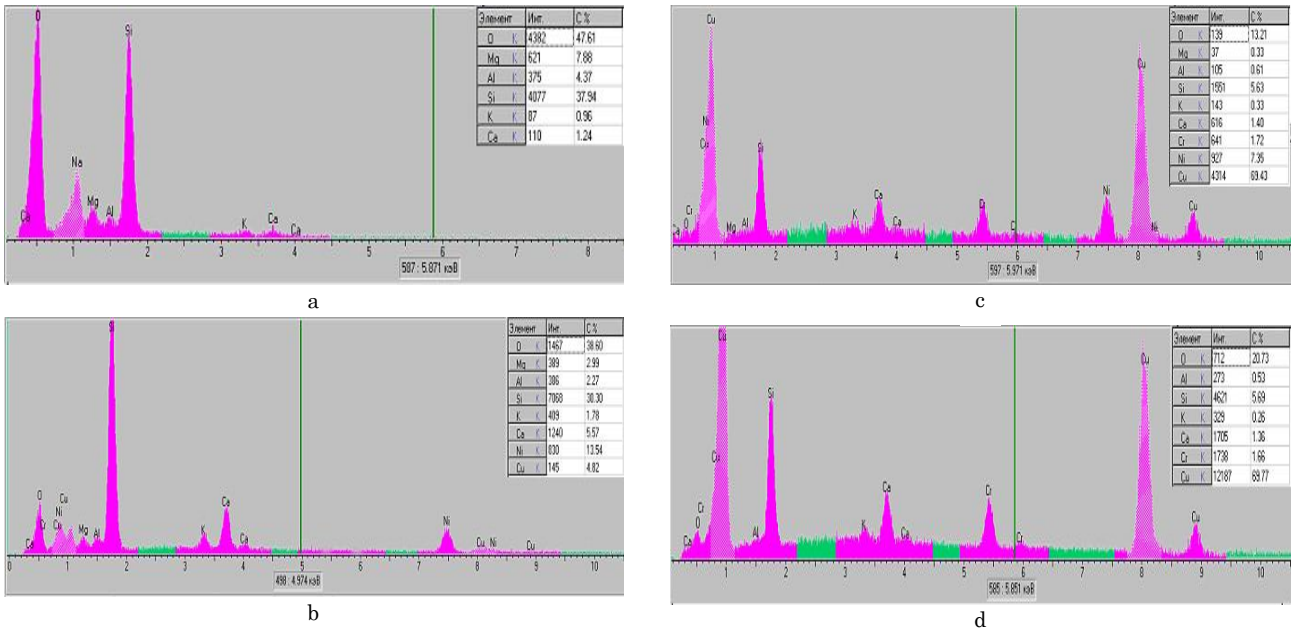

Fig. 3 – Characteristic X-ray spectra of the surface of a glass plate (a), the surface of a film on a glass substrate (b), the surface of a film on a contact pad (c), the surface of a contact pad (d)

The left-hand side of the characteristic X-ray spectrum (Fig. 3 b, c, d) represents the characteristic X-ray emission corresponding to the composition of the glass substrate (Fig. 3 a), since the X-ray generation depth during sample probing with a 20 keV electron beam is on the order of several microns [11], which is much greater than the thickness of the studied films and contact pads. The right-hand side of the spectrum corresponds to the composition of the alloy film sample (Fig. 3 b, c) and the contact pad (Fig. 3 d). The analysis results indicate a relatively high purity of the film samples (absence of impurity atoms of other metals).

The geometric dimensions (length b, width a) of the film (see Fig. 1) were determined by holes machined with high precision in mechanical masks made of nichrome foil. A thin dielectric layer (SiO_2) was pre-applied to the surface of the mask in contact with the substrate as an insulator. The mask was firmly secured to the substrate holder and adhered tightly to the surface of the glass substrate. This ensured consistent film sample sizes across all experiments.

The electrical resistance of the samples during condensation and thermal stabilization in the temperature range of 300-700 K was measured using a V7-34A universal digital voltmeter with an accuracy of 0.01 Ohm (0.1 Ohm for films with resistance greater than 100 Ohm).

The film resistivity ρ was calculated using the geometric dimensions a and b, the film thickness d, and its electrical resistance R, as determined by the relationship $\rho = Rdab^{-1}$. The error in calculating the resistivity was determined primarily by the error in measuring the film thickness and was 10-15% for $d < 50$ nm and 5-10 % for $d > 50$ nm.

After condensation, the films were maintained at substrate temperature (T_s) for 30 minutes. Thermal stabilization of the films' physical properties was achieved using a «heating ↔ cooling» scheme at a constant rate of approximately 3 K/min over three cycles in the temperature range of 300-700 K. After this treatment, the temperature dependence of the electrical resistance was reproduced with high accuracy.

The thermal coefficient of resistance (TCR) β was calculated using the $R(T)$ dependences obtained as a result of heat treatment, based on the relationship $\beta = \Delta R/R\Delta T$. Since the geometric dimensions of the film are not taken into account when determining the TCR, its accuracy was higher than that of the specific resistance and depended only on the accuracy of resistance and temperature measurements.

3. RESULTS AND DISCUSSION

The electrical resistance of the film samples was measured using a two-point scheme both during their condensation and during annealing in the temperature range of 300-700 K. Fig. 4 shows typical dependences of the specific electrical resistance ρ of CuNi alloy films with different component concentrations on the thickness during the condensation process.

During the 30-minute post-condensation hold, the electrical resistance of the film samples generally decreased slightly. This is due to a decrease in the film temperature, which had risen uncontrollably during condensation, and possibly to minor structural ordering.

Analyzing the temperature dependence of the resistance of film samples during thermal stabilization of their electrical properties is extremely important, since the temperature dependences of resistance over several cycles can be used to assess the quality of the heat treatment performed on the samples and the degree of perfection of their structure.

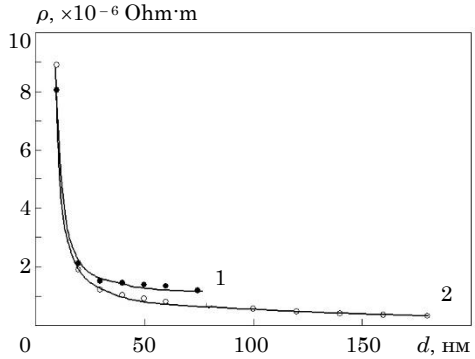

Fig. 4 – Dependences $\rho(d)$ of CuNi alloy films obtained in the condensation process: d = 71 nm, C_{Cu} = 18 at.% (1); d = 179 nm, C_{Cu} = 62 at. % (2)

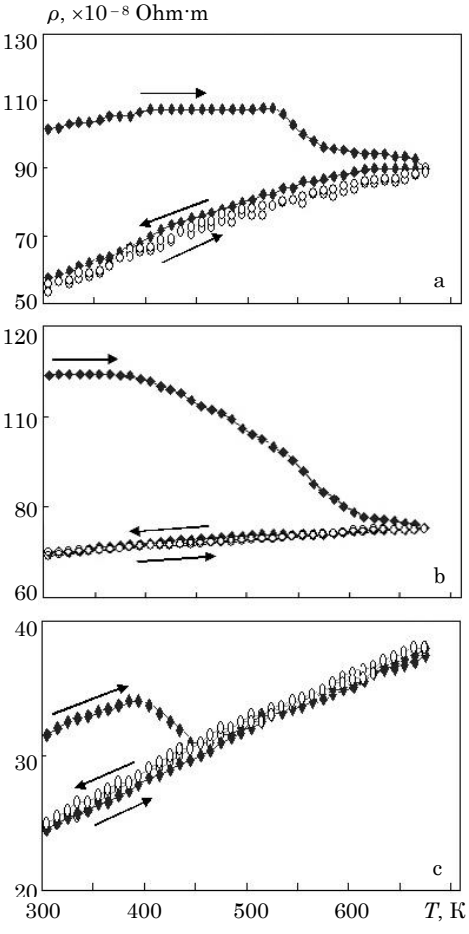

Fig. 5 – Dependence of the specific resistance of CuNi alloy films on temperature during thermal stabilization according to the «heating↔cooling» scheme: d = 85 nm, C_{Cu} = 20 at.% (a); d = 75 nm, C_{Cu} = 40 at.% (b); d = 70 nm, C_{Cu} = 91.5 at. % (c)

Typical dependences of specific resistance on temperature over three «heating ↔ cooling» cycles are shown in Fig. 5 for CuNi alloy films of approximately the same

thickness but different compositions. As can be seen from Fig. 5, during heating in the first cycle, the $\rho(T)$ dependence is non-monotonic.

For all studied samples, an initial slight increase in resistance with increasing temperature was observed, followed by a significant decrease in resistance, atypical for metals, with increasing annealing temperature, after which the metallic $\rho(T)$ dependence reappeared. The decrease in specific resistance with increasing temperature in the second section of the $\rho(T)$ curve is explained by the healing of crystal structure defects in freshly condensed film samples during the annealing process [8].

The $\rho(T)$ dependence on the cooling curve for the first cycle, as well as for the second and third annealing cycles, is monotonic: the resistance increases with increasing temperature. Moreover, the $\rho(T)$ curves during heating and cooling are very close or coincide, indicating complete stabilization of the film samples' properties in this temperature range after the second annealing cycle. The resistance in thermally stabilized films was always lower (by a factor of 1.1-1.4) compared to freshly condensed films, depending on the component concentration.

Fig. 6 shows the temperature dependences of the resistivity for copper-nickel alloy films of approximately the same thickness, d = 150 nm (C_{Ni} = 21 at. %) (Fig. 6 a) and d = 160 nm (C_{Ni} = 27 at.%) (Fig. 6 b), obtained during the first and two subsequent annealings.

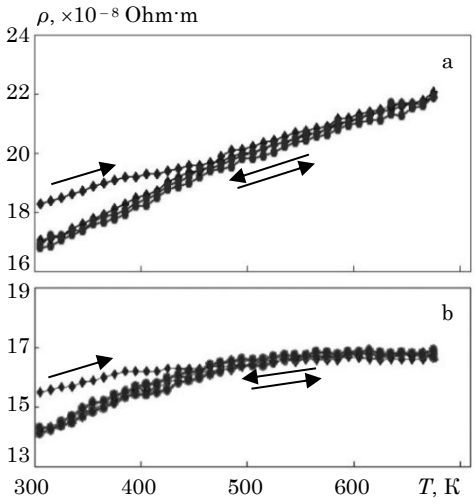

Fig. 6 – Dependences $\rho(T)$ for CuNi alloy films: d = 150 nm, C_{Ni} = 21 at. % (a); d = 160 nm, C_{Ni} = 27 at. % (b)

A peculiarity of these dependences is that during the first annealing practically no irreversible decrease in the specific electrical resistance is observed. The reason for this is obviously that for thicker films (d = 150-160 nm) the improvement of the structure (healing of defects, growth of crystallites, etc.) occurs directly during the condensation process and their moderate annealing up to 700 K practically does not change the structure of the samples. The TCR values of these films are positive and take the values $\beta = 7.4\ 10^{-4}\ K^{-1}$ (Fig. 6 a) and $\beta = 1.2\ 10^{-4}\ K^{-1}$ (Fig. 6 b), which is much less than the TCR values for massive nickel and copper and close to the β_0 values of massive alloys at the same nickel concentrations (see [12, 13]).

It is known that the electrical conductivity of metal films is determined not only by their composition but also by their structure (growth stage) [14]. Moreover, island (granular) films have unique electrophysical properties that differ fundamentally from those of both bulk metal samples and continuous films, approaching those of semiconductors. Their specific electrical resistance ρ is many orders of magnitude higher than that of continuous (thick) films, and the thermal coefficient of resistance β is often negative. An exponential dependence of electrical resistance on temperature is observed, indicating an activation mechanism for electrical conductivity [15].

As already noted, during the thermal stabilization of the electrical properties of structurally continuous CuNi alloy films, an irreversible decrease in resistance was observed in some regions of the temperature dependence of specific resistance. Significant changes in resistance during the first annealing are characteristic of freshly condensed samples and are due to the healing of structural defects [8]. Understanding the defect healing mechanism and the processes that occur during this process is important for interpreting the obtained results on the temperature dependence of resistance. Therefore, we studied the healing of crystal structure defects during film annealing using the «heating ↔ cooling» scheme. Before analyzing the obtained results, we will briefly review the basic tenets of Wend's theory [8], which describes these processes.

According to Wend, for the recombination of structural defects to begin, an energy E must be expended, which ranges from zero to the self-diffusion energy (Q_1) of the film material's atoms. If we denote by $r(E)$ the contribution to the residual resistance due to the formation of one defect per unit volume, then the total specific resistance due to the presence of defects can be written as [8]:

$$\rho_i = \int_{(E)} r(E)N(E,t)dE \tag{3.1}$$

where t is the annealing time required to reach the temperature T at which ρ_i is measured; $N(E, t)$ is the number of defects per unit volume with healing energy from E to $E + \Delta E$.

The value of $N(E, t)$ is found from the relation:

$$\frac{dN(E,t)}{dt} = -cN(E,t)\,exp\left(-\frac{E}{kT}\right) \tag{3.2}$$

where k is the Boltzmann constant.

The coefficient $c = 4\omega_{max}/2\pi$ (n is the number of atoms forming the defect, estimated to be approximately 10 [8]; $\omega_{max} = k\Theta_D/\hbar$ is the maximum frequency of thermal vibrations of the crystal lattice atoms, associated with the Debye temperature of the film Θ_D). In his theory, Wend assumes that Θ_D is equal to the Debye temperature of the bulk sample Θ_{0D}, although according to some experimental data (see, for example, [12, 13]), this temperature depends on the thickness of the sample.

The quantities $r(E)$ and $N(E, t)$ are associated with the defect distribution function, which can be represented as follows:

$$F_0(E) = r(E)N(E,t). \tag{3.3}$$

The function $F_0(E)$ is also related to the specific resistance of the film by a relation that has the following form:

$$F_0(E) = -\frac{1}{kU}\frac{\partial \rho_i}{\partial T} \quad (3.4)$$

where

$$U = \frac{n(u+2)}{u+1}$$

The value of u is determined from the equation

$$u + lg\, u = lg\, \frac{4nt\omega_{max}}{2\pi},$$

$$E = ukT,$$

$$\frac{\partial \rho_i}{\partial T} = \frac{\partial \rho}{\partial T} - \frac{\partial \rho_T}{\partial T}$$

$\frac{\partial \rho}{\partial T}$ and $\frac{\partial \rho_T}{\partial T}$ are the changes in the specific resistance of the film during the first and second annealing.

Plotting the dependence of F_0 on E yields a spectrum of defects caused by deformations in a thin film. The dependence $F_0(E)$ has the form of a curve with one or more maxima corresponding to the activation energy of defect healing, E_m. The contribution to the total resistance of those defects that have a healing energy from E_1 to E_2 can be determined by calculating the area under the curve.

$$\int_{E_1}^{E_2} F_0(E)dE. \quad (3.5)$$

The energy resolution of the method is on the order of kT.

We used the temperature dependences of the resistivity of CuNi alloy films during the first and second thermal stabilization cycles (Fig. 5) to calculate the parameters of structural defects in the samples based on Wend's theory. This resulted in the determination of defect distribution functions, $F_0(E)$, whose numerical value is proportional to the defect concentration in the film. To obtain the defect distribution functions, $F_0(E)$, we calculated the derivative $\frac{\partial \rho}{\partial T}$ at successive annealing temperatures and times, as well as the value taking $\frac{\partial \rho_i}{\partial T}$ into account the second heating. When calculating the defect spectrum, it is necessary to know the Debye temperature (Θ_D) of the samples, which differs slightly from the Θ_{0D} values for the bulk state. In our case, we used the calculated Θ_D value as the average between Θ_{0D}^{Ni} and Θ_{0D}^{Cu}, i.e.

$$\Theta_D = C_{Ni}\Theta_{0D}^{Ni} + (1 - C_{Ni})\Theta_{0D}^{Cu}.$$

It should be noted that although this method for determining the Θ_D of alloys is generally accepted, the accuracy of the calculations is determined by the closeness of the Θ_{0D} values for individual components. Table 1, as an example of the calculation, shows the dependence of Θ_D on concentration for CuNi alloy films with a constant thickness in the range of 70-77 nm.

The resulting Θ_D values were plotted on the thermal stabilization annealing graphs (Fig. 7). As can be seen, the onset of defect annealing occurs at a temperature of $T \approx \Theta_D$.

Typical dependences of the defect distribution function F_0 on the energy E for film alloys with different component concentrations are shown in Fig. 8.

Table 1 – Dependence of Θ_D of CuNi alloy films on the concentration of components

d, nm	C_{Cu}, at.%	Θ_D, K
bulk Ni [12]	0	465
71	19	441
77	37	418
76	45	408
74	52	399
70	60	389
70	80,5	365
75	85	358
bulk Cu [12]	100	339

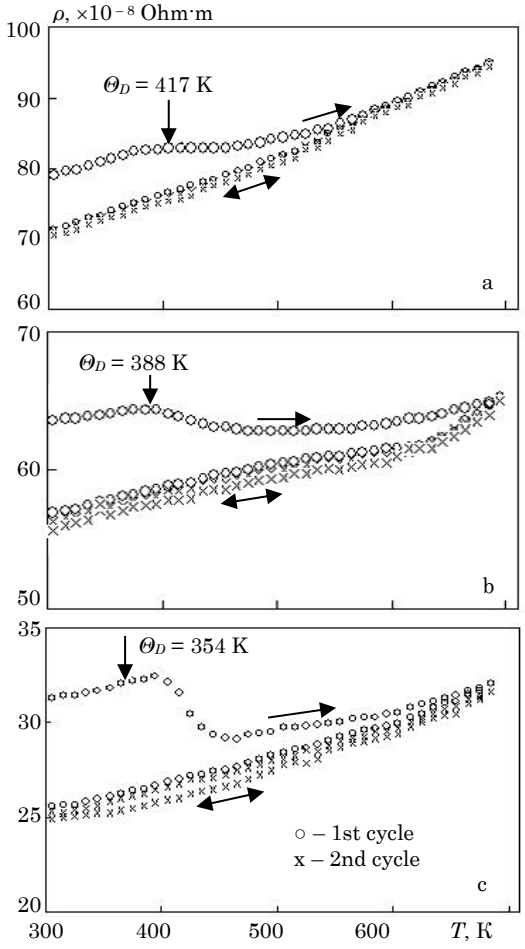

Fig. 7 – Temperature dependence of the resistivity of CuNi alloy films of the same thickness d = 55 nm with different component concentrations. Copper concentration, at.%: 38 (a); 61 (b); 88 (c)

Note that at high concentrations of Ni atoms, the energy dependences of the distribution function for CuNi films exhibit two maxima with healing energies E_{m1} = 0.46-0.51 eV and E_{m2} = 0.58-0.64 eV (Fig. 8 a). These maxima are well described by a Gaussian distribution, and the half-width of the maxima (up to 0.12 eV) is in good agreement with the conclusions of Wend's theory [8].

Indeed, according to this theory, the deformation of the crystal lattice with a constant annealing energy should be

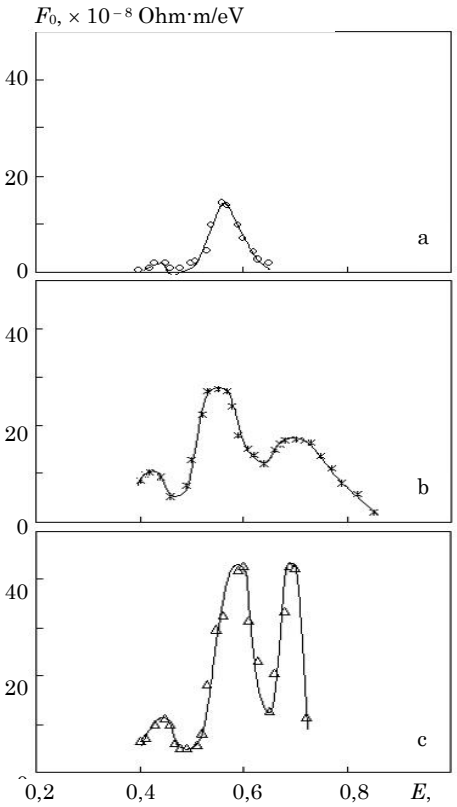

Fig. 8 – Distribution function of defects F_0 on energy for CuNi film alloys (d = 60 nm, $\omega \approx$ 0.5-1.5 nm/s). Copper concentration, at. %: 24 (a); 65 (b); 71 (c)

reproduced as a diffuse curve with a width of about $2kT$. At an annealing temperature of 700 K, this half-width is 0.11 eV, which was observed experimentally. With increasing copper atom concentration in CuNi alloy films, an additional peak appears in the crystal structure defect spectrum, with the defect healing activation energy shifted to higher energies, E_{m3} = 0.70-0.75 eV. This peak is the result of the onset of a new annealing stage for defects with higher activation energies. Since the height of this peak increases with increasing copper concentration in the samples (Fig. 8 b-c), this indicates an increase in the number of structural defects caused by the increasing number of copper atoms occupying «incorrect» positions in the crystal lattice during film condensation (higher-temperature annealing of such samples stimulates their ordering).

According to Wend's theory, the defect healing mechanism in freshly condensed samples is associated with a combined vacancy-interstitial atom defect. Based on the analysis of experimental results by various authors, it can be concluded that the main defects in the crystal structure of pure metal films are the «vacancy – impurity atom from the residual atmosphere» complex, and only in some cases – combined «vacancy – interstitial atom» defects. Indeed, to initiate the healing process, it is necessary to expend energy close to the self-diffusion energy of the film material atoms Q_1, which for bulk Cu and Ni is 2.05 eV and 2.9 eV, respectively [14, 16]. A comparison of the values of Q_1 and E_m shows that the self-diffusion energy exceeds the activation energy by 3-4 times. The activation energy for the diffusion of gas atoms in the metal crystal lattice Q_2 in most cases does not exceed 1 eV [17]. Since in the case of CuNi alloy films, as for single-component films, the activation energy E_m is commensurate with Q_2, it can be assumed that in freshly condensed samples, healing of the «vacancy – impurity atom from the residual atmosphere» defects occurs. This does not contradict the data on the increase in the lattice parameter due to the absorption of atoms from the residual atmosphere (see [9]).

4. CONCLUSIONS

1. The temperature dependences of the specific electrical resistance $\rho(T)$ of CuNi alloy films for the second and subsequent heating-cooling cycles are virtually identical, indicating complete stabilization of the film sample properties after the second annealing cycle.

2. Using the Wend method, the spectra of crystal structure defects in as-condensed CuNi alloy films were calculated.

3. The observed maxima with defect healing activation energies less than 1 eV belong, in most cases, to the «vacancy – impurity atom from the residual atmosphere» complex.

REFERENCES

1. V.K. Soni, S. Sanyal, S.K. Sinha, *Vacuum* **174**, 109173 (2020).
2. G. Li, G. Song, N. Wang, *Surf. Interface* **28**, 101651 (2022).
3. P.H. Wu, N. Liu, W. Yang, Z.X. Zhu, Y.P. Lu, X.J. Wang, *Mater. Sci. Eng.: A* **642**, 142 (2015).
4. Yu.O. Shkurdoda, A.M. Chomous, Yu.M. Shabelnyk, L.V. Dekhtyaruk, V.B. Loboda, S.M. Khursenko, *10th International Conference on Nanomaterials Applications and Properties (NAP-2020)*, art. no. 9309616 (Sumy: Sumy State University: 2020).
5. A.D. Pogrebnjak, Y. Bing, M. Sahul, *Nanocomposite and Nanocrystalline Materials and Coatings. Microstructure, Properties and Applications*, 236 (Singapore: Springer: 2024).
6. S. I. Protsenko, I. V. Cheshko, D. V. Velykodnyj, I. V. Pazukha, L. V. Odnodvorets, I. Yu. Protsenko, O. V. Synashenko, *Progress in Physics of Metals* **8**, *247* (2007).
7. Yu. Shabelnyk, I. Protsenko, P.K. Mehta, L. Odnodvorets, Ch. Panchal, K. Tyshchenko, N. Shumakova, *J. Nano- Electron. Phys.* **6** No 1, 01031 (2014).
8. V. Vand, *Proc. Phys. Soc.* **55** No 3, 222 (2002).
9. V.B. Loboda, S.M. Khursenko, V.O. Kravchenko, *Adv. Struct. Mater.* **214**, 201 (2024).
10. V.B. Loboda, V.M. Zubko, S.M. Khursenko, V.O. Kravchenko, A.V. Chepizhnyi, *J. Nano- Electron. Phys.* **15** No 5, 05014 (2023).
11. J.I. Goldstein, D.E. Newbury, P. Echlin, D.C. Joy, C.E. Lyman, E. Lifshin, J.R. Michael, *Scanning Electron Microscopy and X-ray Microanalysis* (New York: Springer Science + Business Media: 2003).
12. W. Benenson, J.W. Harris, H. Stocker, H. Lutz, *Handbook of Physics* (New York: Springer-Verlag: 2002).
13. W.M. Haynes, *Handbook of Chemistry and Physics* (Boca Raton: CRC Press: 2017).
14. H. Frey, H.R. Khan. *Handbook of Thin-Film Technology* (Berlin: Springer-Verlag: 2015).
15. S.V. Tomilin, V.N. Berzhansky, E.T. Milyukova, O.A. Tomilina, A.S. Yanovsky, *Phys. Solid State* **60** No 7, 1255 (2018).
16. W.F. Gale, T.C. Totemeier, *Smithells Metals Reference Book* (Heinemann: Elsevier Butterworth: 2004).
17. N.T. Gladkikh, Poverkhnostnyye Yavleniya i Fazovyye Prevrashcheniya v Kondensirovannykh Plenkakh, 276 (Kharkov: KhNU im. V.N. Karazina: 2004) [In Russian].

Електропровідність тонких плівок мідно-нікелевих сплавів

В.Б. Лобода, С.М. Хурсенко, В.О. Кравченко, В.М. Зубко

Сумський національний аграрний університет, 40021 Суми, Україна

У цій роботі представлені результати дослідження електропровідності структурно суцільних нанокристалічних плівок сплавів CuNi в широкому інтервалі товщин і концентрацій компонент. Плівки сплавів товщинами 50-200 нм були отримані одночасним роздільним випаровуванням компонент (мідь та нікель) у вакуумі 10^{-4} Па. Мідь випаровувалася зі стрічки з вольфрамової фольги завтовшки 0,05 мм. Нікель випаровувався електронно-променевим способом за допомогою електронної діодної гармати. Швидкість конденсації становила 0,5-1,5 нм/с. Чистота випаровуваних металів становила щонайменше 99,98 %. Залежності питомого електроопору від температури плівок сплавів CuNi для другого і наступних циклів «нагрівання-охолодження» практично збігаються, що свідчить про повну стабілізацію властивостей плівкових зразків вже після другого циклу відпалювання. Для пояснення специфічного незворотного зменшення величини електроопору в процесі термостабілізації електрофізичних властивостей плівок сплавів CuNi нами була використана модель Венда, що описує залікування дефектів кристалічної структури плівок. На основі цієї моделі було розраховано спектри дефектів кристалічної структури у плівках сплавів CuNi.

Ключові слова: Тонкі плівки, Нанокристалічні плівки, Сплави, Електропровідність, Дефекти кристалічної структури, Енергія активації залікування дефектів.